Defense Technical Information Center Compilation Part Notice

ADP011221

TITLE: Determination of a Quantitative Algorithm for the Measurement of Muscle Oxygenation Using CW Near-Infrared Spectroscopy Mean Optical Pathlength Without the Influence of Adipose Tissue

DISTRIBUTION: Approved for public release, distribution unlimited

This paper is part of the following report:

TITLE: Optical Sensing, Imaging and Manipulation for Biological and Biomedical Applications Held in Taipei, Taiwan on 26-27 July 2000. Proceedings

To order the complete compilation report, use: ADA398019

The following component part numbers comprise the compilation report:
ADP011212 thru ADP011255

Determination of a quantitative algorithm for the measurement of muscle oxygenation using CW near-infrared spectroscopy —Mean optical pathlength without the influence of adipose tissue—

Jun Shao[a], Ling Lin[b], Masatsugu Niwayama[a],
Nobuki Kudo[a], and Katsuyuki Yamamoto[*a]

[a]Division of Biomedical Systems Engineering, Graduate School of Engineering,
Hokkaido Univ., North 13 West 8, Sapporo 060-8628, Japan
[b]College of Precision Instruments and Optoelectronics Engineering,
Tianjin University, Tianjin 300072, P. R. China

ABSTRACT

Near-infrared spectroscopy (NIRS) is a useful technique for noninvasive measurement of oxygenation of the brain and muscle. However, no accurate, quantitative algorithms for continuous wave NIRS (CW-NIRS) have yet been presented dute to the following two problems. The first is that inhomogeneous tissue structure greatly affects measurement sensitivity. We previously reported on the influence of a fat layer on muscle oxygenation measurement and proposed a method for correcting the sensitivity. The second problem is that almost all algorithms for CW-NIRS have been experimentally determined, although an algorithm can be theoretically determined on the basis of diffusion theory if the mean optical pathlength in muscle in an *in vivo* state is known. In this study, we derived basic equations for a CW-NIRS algorithm based on diffusion theory, and we determined linear and nonlinear algorithms from mean optical pathlengths and validated them by results obtained from phantom experiments. For the determination of pathlength, the absorption and scattering coefficients of the muscle must be obtained *by taking into account the influence of a fat layer*. Laser pulses of 752 and 871 nm were applied to the forearms of subjects, and the temporal point spread function (TPSF) was obtained by using a streak camera. The absorption and scattering coefficients of the muscle were determined by fitting the measured TPSF with that obtained by a Monte Carlo model consisting of skin, fat and muscle layers. From these coefficients, the mean optical pathlengths at two wavelengths were obtained and the algorithms were determined.

Keywords: NIRS, tissue oximeter, muscle, hemoglobin concentration, mean optical pathlength, time resolved spectroscopy

1. INTRODUCTION

In recent years, near-infrared spectroscopy (NIRS) has been used clinically as a noninvasive method for measuring tissue oxygenation. Among various techniques for NIRS, continuous wave (CW) NIRS is the simplest technique and it can be easily be applied to real-time monitoring, including a mapping system of tissue oxygenation. However, CW-NIRS only enables measurement of the relative change in oxygenation from an initial level. There have been many efforts to determine the absolute value of oxygenation using time-resolved spectroscopy, spatially resolved spectroscopy, and intensity modulated spectroscopy. However, even if these techniques are used to measure tissue oxygenation, quantitative measurement is difficult because of the inaccurate assumption that tissue is homogeneous.

Overlying tissues such as the skull and subcutaneous adipose tissue greatly affect the measurement sensitivity of NIRS. Therefore, changes in oxygenation, even from the initial level, can not be compared among subjects. As for muscle oxygenation measurement, Homma *et al.*[1] showed the influence of a fat layer by *in vivo* experiments using CW-NIRS. We [2-5] have also verified from the results of *in vivo* measurements and Monte Carlo simulation that a strong correlation exists between fat layer thickness and measurement sensitivity. Based on the results of analyses of the influence of a fat layer, we have developed correction methods for measurement sensitivity using a detected light intensity or correction curves. After correcting the measurement sensitivity, we are able to obtain the change in absorption using an algorithm that assumes homogeneity of tissue.

[*]Correspondence: E-mail: yamamoto@bme.eng.hokudai.ac.jp; Phone: +81-11-706-6763; Fax: +81-11-706-7802

In *Optical Sensing, Imaging, and Manipulation for Biological and Biomedical Applications*, Robert R. Alfano, Ping-Pei Ho, Arthur E. T. Chiou, Editors, Proceedings of SPIE Vol. 4082 (2000) • 0277-786X/00/$15.00

Most algorithms used for CW-NIRS are based on the modified Beer-Lambert law[6], which assumes that the change in optical density is proportional to the change in absorption and that the proportional constant, mean optical pathlength, does not greatly vary when the change in absorption is small. Delpy and his group obtained a theoretical equation for determining this pathlength from a temporal point spread function (TPFS)[6]. However, an analytical solution, based on CW theory, for the determinations of the mean optical pathlength and the coefficients of an algorithm is not available. Furthermore, different algorithms that are experimentally determined are used at present and therefore these algorithms result in inconsistent measurements as pointed out by Matcher[7].

In the present study, we theoretically derived algorithms, based on diffusion theory, for continuous wave (CW) spectroscopy to determine the change in tissue oxygenation and the algorithms were validated by the results of phantom experiments. The relationship between change in optical density and change in absorption is essentially nonlinear; therefore, algorithms with and without consideration of the nonlinear relationship were derived. Since the optical properties of muscle must be determined for obtaining the algorithms, we also measured absorption and scattering coefficients of muscle from a TPSF *by taking into account the influence of an overlying fat layer.*

2. THEORETICAL DERIVATION OF THE ALGORITHMS

2.1. Tissue oximetry with CW light

In NIRS, back-scattered light is detected at a distance from a light source, and tissue oxygenation is determined from the change in absorption coefficients of a tissue using a basic equation of conventional oximetry. Assuming that the change in absorption is mostly due to the change in blood oxygenation or volume, changes in the concentrations of oxy-hemoglobin ΔHbO_2 and deoxy-hemoglobin ΔHb can be determined as follows.

Change in the absorption coefficient of a tissue $\Delta\mu_a$ is expressed as

$$\Delta\mu_a = \varepsilon_\lambda^{\mathrm{HbO_2}} \Delta HbO_2 + \varepsilon_\lambda^{\mathrm{Hb}} \Delta Hb, \tag{1}$$

where $\varepsilon_\lambda^{\mathrm{HbO2}}$ and $\varepsilon_\lambda^{\mathrm{Hb}}$ are molar extinction coefficients of HbO_2 and Hb at a wavelength of λ, respectively. The two unknowns, ΔHbO_2 and ΔHb, can be determined by solving simultaneous equations, which are obtained from measurements at two wavelengths.

$$\Delta HbO_2 = \frac{1}{k}\left(\varepsilon_2^{\mathrm{Hb}} \Delta\mu_{a1} - \varepsilon_1^{\mathrm{Hb}} \Delta\mu_{a2}\right), \tag{2}$$

$$\Delta Hb = \frac{-1}{k}\left(\varepsilon_2^{\mathrm{HbO_2}} \Delta\mu_{a1} - \varepsilon_1^{\mathrm{HbO_2}} \Delta\mu_{a2}\right), \tag{3}$$

$$k = \varepsilon_1^{\mathrm{HbO_2}} \varepsilon_2^{\mathrm{Hb}} - \varepsilon_1^{\mathrm{Hb}} \varepsilon_2^{\mathrm{HbO_2}}, \tag{4}$$

where the subscripts 1 and 2 indicate the wavelengths. The change in absorption $\Delta\mu_a$ is determined by various NIRS techniques; i.e., CW, spatially resolved, intensity-modulated and time-resolved spectroscopy. The CW method, which is the simplest, only enables determination of the change in absorption, whereas corresponding optical properties of absolute values can be obtained by using the other techniques. However, it is difficult to eliminate the effects of absorption other than that of hemoglobin, such as absorption of myoglobin. Therefore, only $\Delta\mu_a$ is usually measured in NIRS, assuming that the change in optical properties is only due to blood.

In CW-NIRS, change in optical density defined by $\Delta OD=\ln(R_0/R)$, where R_0 and R are intensities of back-scattered light at a reference state (usually taken at the start of measurement) and during the measurement, respectively, is measured. Assuming that the scattering coefficient does not change during the measurement, we can determine $\Delta\mu_a$ using the modified Beer-Lambert law[6].

$$\Delta OD = \Delta\mu_a d\,, \tag{5}$$

where d is $d = \partial\,\mathrm{OD}/\partial\,\mu_a$, which is defined as the differential pathlength and is equal to the mean optical pathlength[6]. In the next section, we will present a theoretical equation for determining d, based on CW theory.

2.2. Derivation of an algorithm based on linear approximation

Intensity of back-scattered light $R(\rho)$ at a distance ρ from a CW light source in a semi-infinite medium is given by the following solution[8], which is obtained from the optical diffusion equation.

$$R(\rho) = \frac{1}{a\mu_t'}\left(\mu_{eff} + \frac{1}{\rho}\right)\frac{e^{-\mu_{eff}\rho}}{\rho^2}\,, \tag{6}$$

$$\mu_t' = \mu_a + \mu_s'\,, \tag{7}$$

$$\mu_{eff} = \sqrt{3\mu_a(\mu_a + \mu_s')}\quad, \tag{8}$$

where a is a constant. From equation (6), the change in optical density (base e) is given by

$$\Delta OD = \ln\frac{R_0(\rho)}{R(\rho)} = \rho\left(\mu_{eff} - \mu^0{}_{eff}\right) - \left\{\ln\left(1+\rho\mu_{eff}\right) - \ln\left(1+\rho\mu_{eff}^0\right)\right\}, \tag{9}$$

where $R_0(\rho)$ and μ_{eff}^0 are $R(\rho)$ and μ_{eff} in a reference state, respectively. Since it holds in tissues that $\mu_a << \mu_s'$, μ_{eff} can be approximated by

$$\mu_{eff} = \sqrt{3\mu_a(\mu_a + \mu_s')} \approx \sqrt{3\mu_a\mu_s'}\,. \tag{10}$$

From the definition of a differential pathlength and equations (9) and (10), mean optical pathlength d is derived as follows.

$$d = \frac{\partial\Delta OD}{\partial\mu_a} = \frac{\partial\Delta OD}{\partial\mu_{eff}}\frac{\partial\mu_{eff}}{\partial\mu_a} = \frac{\rho^2\mu_{eff}}{1+\rho\mu_{eff}}\frac{3\mu_s'}{2\sqrt{3\mu_a\mu_s'}} = \rho'\frac{3\mu_s'}{2\mu_{eff}} = \rho'\frac{\mu_{eff}}{2\mu_a}\,, \tag{11}$$

$$\rho' = \frac{\rho^2\mu_{eff}}{1+\rho\mu_{eff}}\,. \tag{12}$$

According to equation (11), d depends on the optical properties of a tissue. In actual measurement, μ_s' can be regarded as a constant, but μ_a changes. Thus, equation (5) does not strictly hold but is linearly approximated around an operating point on the assumption that the change in μ_a is small. When the linear approximation is valid, we can obtain the following theoretical algorithm for the determination of ΔHbO_2 and ΔHb from equations (2) to (5).

$$\Delta HbO_2 = \frac{1}{k}\left(\frac{\varepsilon_2^{\mathrm{Hb}}\Delta OD_1}{d_1} - \frac{\varepsilon_1^{\mathrm{Hb}}\Delta OD_2}{d_2}\right), \tag{13}$$

$$\Delta Hb = \frac{-1}{k}\left(\frac{\varepsilon_2^{\mathrm{HbO_2}}\Delta OD_1}{d_1} - \frac{\varepsilon_1^{\mathrm{HbO_2}}\Delta OD_2}{d_2}\right), \tag{14}$$

where d_1 and d_2 are mean optical pathlengths determined by equation (11) at wavelengths 1 and 2, respectively. These equations are similar to conventional ones used for two-wavelength transmission spectroscopy, in which $d=d_1=d_2$, but this does not hold in a reflection method. Moreover, d_1 and d_2 should be determined with consideration to the absorption of

tissue other than that of blood. In other words, the mean optical properties of measured tissue around an operating point (in a reference state) are necessary for the determination of d_1 and d_2. If these pathlengths are known, coefficients of the algorithm can be determined.

2.3. Nonlinear algorithm

The calculation error of the linear approximation can not be ignored when $\Delta\mu_a$ is large. In this section, we derive theoretical equations that take into account the nonlinear relationship between optical density and absorption. The equation that we need is a function of ΔOD that gives $\Delta\mu_a$. Since equation (9) is an implicit function of μ_{eff}, which is a function of μ_a, some approximation is needed in order to derive the algorithm. Taylor expansion gives the following relationship when we ignore the high-order terms above the second derivative; the second-derivative term was less than 2% of the first-derivative one, as confirmed by substituting typical values into each term, assuming that μ_{eff} increases by 50%.

$$\begin{aligned}\Delta OD &\approx \Delta OD\ (\mu_{eff}^0) + \frac{\partial \Delta OD}{\partial \mu_{eff}} \Delta\mu_{eff} \\ &= \rho \Delta\mu_{eff} - \frac{\rho \Delta\mu_{eff}}{1+\rho\mu_{eff}^0} \\ &= \frac{\rho^2 \mu_{eff}^0}{1+\rho\mu_{eff}^0} \Delta\mu_{eff} \\ &= \rho' \Delta\mu_{eff}\end{aligned} \quad . \tag{15}$$

This equation means that ΔOD is not proportional to $\Delta\mu_a$ but simply proportional to $\Delta\mu_{eff}$. Substituting $\mu_{eff} = \mu_{eff}^0 + \Delta\mu_{eff}$ and $\mu_a = \mu_a^0 + \Delta\mu_a$ into equation (10), $\Delta\mu_a$ can be expressed by the second-order equation of $\Delta\mu_{eff}$:

$$1 + \frac{\Delta\mu_{eff}}{\mu_{eff}^0} = \sqrt{1 + \frac{\Delta\mu_a}{\mu_a^0}}\ , \tag{16}$$

$$\Delta\mu_a = \left\{ 2\frac{\Delta\mu_{eff}}{\mu_{eff}^0} + \left(\frac{\Delta\mu_{eff}}{\mu_{eff}^0} \right)^2 \right\} \mu_a^0 . \tag{17}$$

From equations (15) and (17), we obtain

$$\Delta\mu_a = \left(1 + \frac{1}{4\mu_a} \frac{\Delta OD}{d} \right) \frac{\Delta OD}{d} \quad . \tag{18}$$

The first term of this equation is equivalent to equation (5), and the second term represents the nonlinear relationship. The equation for determining ΔHbO_2 and ΔHb can be obtained by substituting the above equation into equations (2) and (3).

$$\Delta HbO_2 = \frac{1}{k} \left(\varepsilon_2^{\mathrm{Hb}} \left(1 + \frac{1}{4\mu_{a1}} \frac{\Delta OD_1}{d_1} \right) \frac{\Delta OD_1}{d_1} - \varepsilon_1^{\mathrm{Hb}} \left(1 + \frac{1}{4\mu_{a2}} \frac{\Delta OD_2}{d_2} \right) \frac{\Delta OD_2}{d_2} \right), \tag{19}$$

$$\Delta Hb = \frac{-1}{k} \left(\varepsilon_2^{\mathrm{HbO_2}} \left(1 + \frac{1}{4\mu_{a1}} \frac{\Delta OD_1}{d_1} \right) \frac{\Delta OD_1}{d_1} - \varepsilon_1^{\mathrm{HbO_2}} \left(1 + \frac{1}{4\mu_{a2}} \frac{\Delta OD_2}{d_2} \right) \frac{\Delta OD_2}{d_2} \right). \tag{20}$$

3. PHANTOM EXPERIMENTS

3.1. Materials and methods

In order to validate the theoretically derived algorithms, we performed phantom experiments using the apparatus shown in Fig. 1. The apparatus consisted of a phantom, a driver and a light source, a detector and an amplifier, and a computer. The construction of this apparatus is only described simply below since it is almost the same as that of a previously reported one[4].

As the light source, a two-wavelength light-emitting diode (LED, 840 and 760 nm) was used. Back-scattered light was detected by a photodiode (Hamamatsu Photonics, S2386-45K) at a distance of 30 mm from the LED. The phantom consisted of 1% Intralipid solution suspended in phosphate-buffered saline (PBS), into which bovine hemoglobin solution was gradually added. The reduced scattering coefficient of the Intralipid suspension was determined by TPSF, which was measured by a pulsed laser (Hamamatsu Photonics, PLP-02, 752 nm) and a streak camera (Hamamatsu Photonics, C4334): $\mu_s' = 0.85\ \text{mm}^{-1}$. The size of the tank for the phantom was $15 \times 14 \times 12.5\ \text{cm}^3$, and the volume of solution used in the experiments was about 1500 ml. Three experiments were conducted under the following conditions.

Experiment 1: The relationship between changes in OD and concentrations of fully oxygenated hemoglobin was obtained. Concentration of hemoglobin solution of the phantom was varied from 0 to 0.1 mM by adding this solution to the phantom in steps of 0.008 mM using a micropipette. Oxygen gas was bubbled into the phantom to ensure full oxygenation, which was confirmed by using a blood gas analyzer (Ciba-Corning, Model 170); the calculated oxygen saturation of hemoglobin was more than 99%.

Experiment 2: The same experiment as that of above was conducted under the condition of a fully deoxygenated state. Five grams of yeast, suspended in the phantom, was used to make a fully deoxygenated state. When the hemoglobin solution was added, the phantom solution was sufficiently stirred to ensure complete oxygen consumption by the yeast. The blood gas analyzer was also used to confirm that a fully deoxygenated state had been achieved.

Experiment 3: Oxygen saturation was varied while the hemoglobin concentration was fixed at 0.054 mM (1% of corresponding hematocrit). The phantom was first bubbled with oxygen gas and then bubbled with nitrogen gas to vary the oxygen saturation of hemoglobin, which was also measured by the blood gas analyzer.

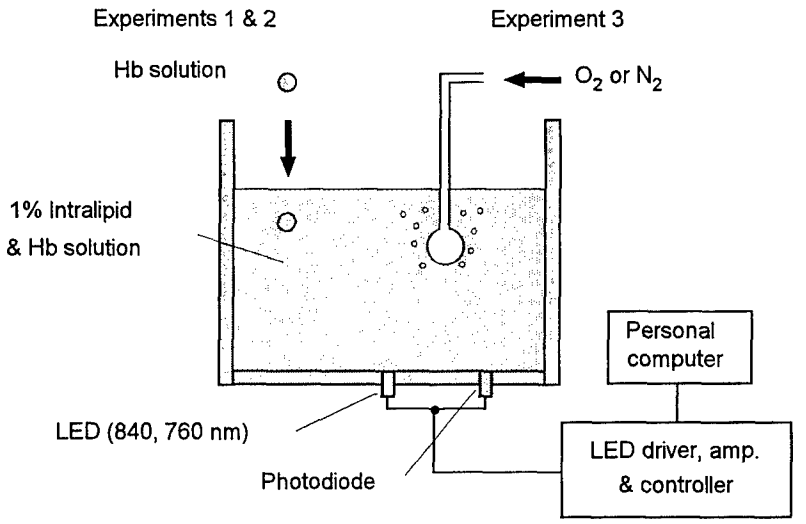

Fig. 1 Experimental apparatus using a tissue-mimic phantom. Changes in optical density with addition of hemoglobin solution were measured under fully oxygenated and deoxygenated states in experiments 1 and 2, respectively. In experiments 3, oxygen saturation was varied while the hemoglobin concentration was fixed.

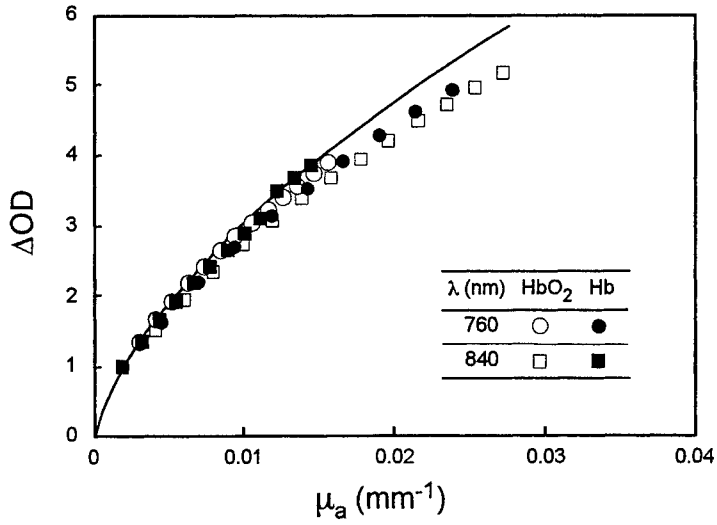

Fg. 2 Relationship between change in optical density and absorption coefficient of the phantom. Results of experiments 1 and 2, denoted by HbO_2 and HB, respectively, were plotted.

3.2. Experimental results

In order to compare the experimental results with the theoretical values, all of the results of experiments 1 and 2 were plotted against the absorption coefficient, which was calculated from the molar extinction coefficient of hemoglobin[7] and its concentration (Fig. 2). Absorption of water (0.003 mm^{-1}) was also taken into account, and the reference state of the change in optical density was set to be theoretically zero in absorption; therefore, the experimental results were shifted upward so that the first point of the plotted results of each experiment before addition of the hemoglobin solution was consistent with the theoretical curve, which is indicated by a solid line. As shown in Fig. 2, the experimental results agreed well with the theoretical curve, which was obtained from equation (9).

3.3 Evaluations of theoretical CW-NIRS algorithms

The algorithms for obtaining ΔHbO_2 and ΔHb, equations (13) and (14) and equations (19) and (20), were evaluated by comparing calculated concentrations with those set in the experiments. When calculating the concentrations, we need the mean optical pathlengths d_1 and d_2 at an operating point in order to determine the coefficients of the algorithm. In the evaluation using the results of experiments 1 and 2, we set the operating point on 0.054 mM of hemoglobin concentration, assuming that equivalent hematocrit of a muscle tissue is 1%. In experiment 3, in which oxygen saturation was varied, we chose 70% saturation as the operating point. The corresponding optical pathlengths for each experiment were thus determined from equations (11) and (12) using absorption and scattering coefficients of the phantom.

Figure 3 shows the results obtained by equations (13) and (14) that were based on linear approximation. The abscissa is the hemoglobin concentration, which was set in experiments 1 and 2 or calculated from oxygen saturation measured in experiment 3. The straight line in each figure is a line of identity. The calculated concentrations agree well with those obtained from the experiments around the operating points. However, in regions far from these points (change in hemoglobin concentration > about 0.02 mM in experiments 1 and 2), significant deviations occurred due to the linear approximation. Compared to this, the calculated concentrations using equations (19) and (20) agreed well with those obtained from the experiments even when there was a large change in absorption, as shown in Fig. 4.

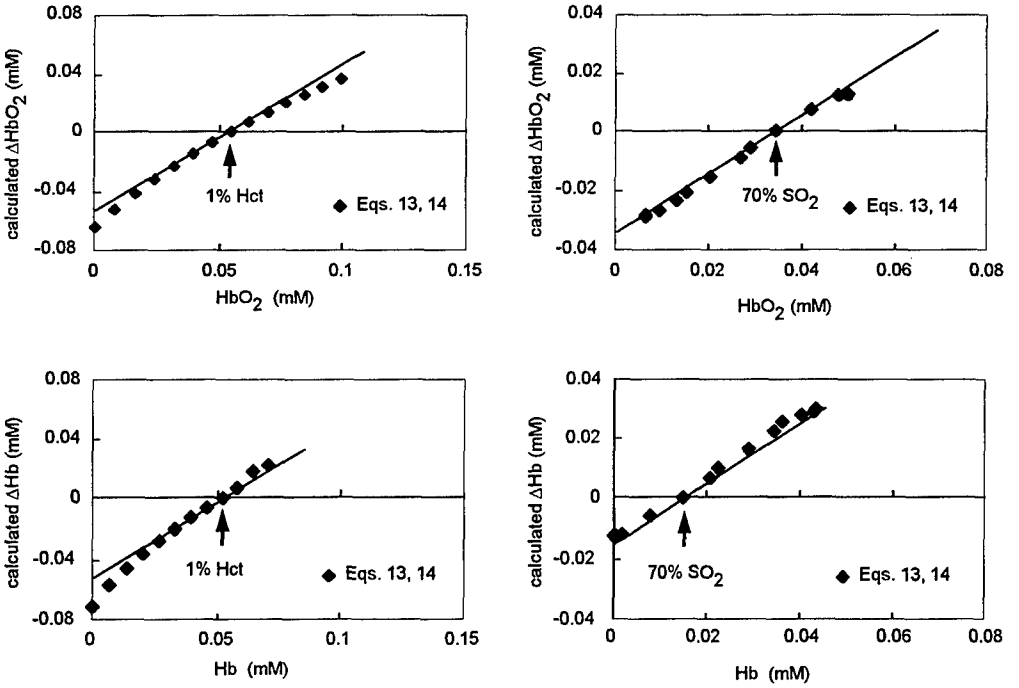

Fig. 3 Changes in hemoglobin concentration calculated from equations 13 and 14. The abscissa is hemoglobin concentration set in the experiments. The straight line in each figure is a line of identity. Upper left: experiment 1; lower left: experiment 2; right: experiment3. Arrows indicate operating points chosen for the calculation.

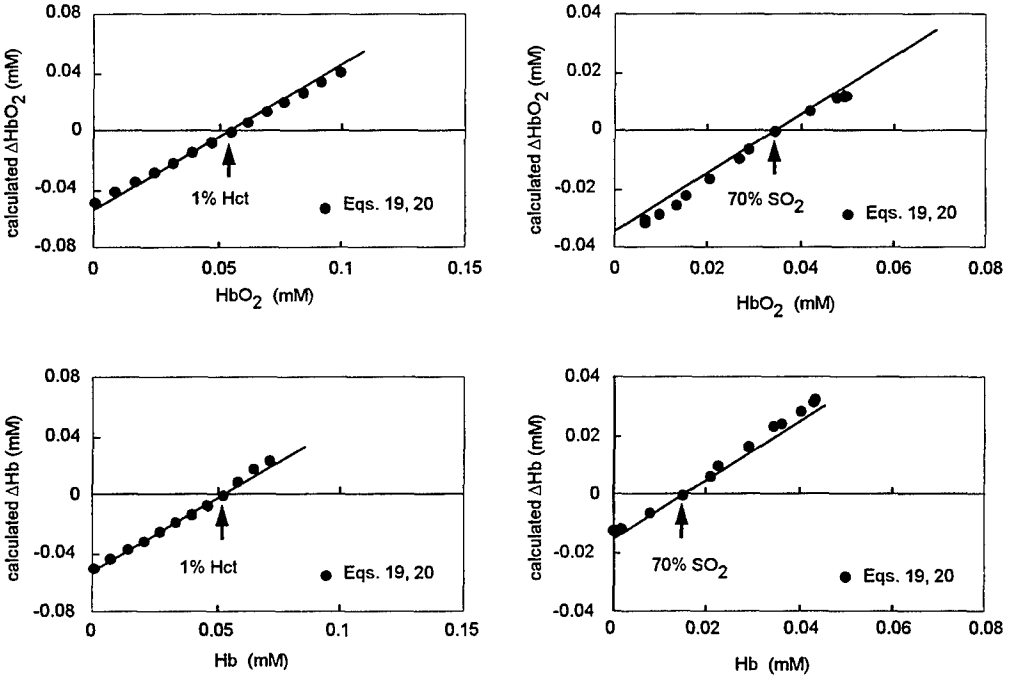

Fig. 4 Changes in hemoglobin concentration calculated from equations 19 and 20. The abscissa is the hemoglobin concentration set in the experiments. The straight line in each figure is a line of identity. Upper left: experiment 1; lower left: experiment 2; right: experiment3. Arrows indicate operating points chosen for the calculation.

4. DETERMINATIONS OF *IN VIVO* OPTICAL PROPERTIES OF MUSCLE AND CW-NIRS ALGORITHM

Our final goal was to determine the coefficients of algorithms that can be applied to *in vivo* measurements. If the absorption coefficient of the muscle does not greatly vary during measurements and among subjects, we can determine coefficients of the algorithms. For accurate determination of pathlength, the optical properties of muscle must be obtained by eliminating the influence of a fat layer. However, there have only been a few studies[9] on these properties.

4.1. Materials and methods

4.1.1. Instrumentation

Pico-second pulsed lasers (Hamamatsu Photonics, PLP-02, 50-ps FWHM, wavelengths of 752 and 871 nm) and a streak camera (Hamamatsu Photonics, C4334) were used to measure the TPSF of back-scattered light from tissues (Fig.5). The optical arrangement is shown in Fig. 4. An optical fiber of 200 μm in core diameter was coupled to the laser, and light pulses were guided to a skin surface. The photons back-scattered from the tissues were collected by an optical fiber bundle of 1.6 mm in diameter and fed into the streak camera. Fibers were arrayed in line at the end of the bundle that was connected to the streak camera; thus, the signal-to-noise ratio was substantially improved. Photons were counted while the pulsed light was emitted at a repetition rate of 1 MHz, and temporal profile data were stored in a computer.

The separation between the source fiber and the detector fiber was 15 mm for adipose measurements on the abdomen and 25 mm for muscle measurements on the forearm. The instrument function was measured after each measurement by placing the source and detector fibers close to each other. To reduce light intensity, an attenuator was placed between both fiber ends. The obtained instrument function was used to deconvolute the measured TPSFs yielding the corrected reflectance.

4.1.2. *In vivo* measurements and data analysis

Measurements on the abdomen were performed to obtain μ_a and μ_s' of adipose tissue in three males, whose fat layer thicknesses of the abdomen were about 20 mm. The fibers were fixed longitudinally with respect to the abdominal wall. A separation of 15 mm of the source-detector fibers was chosen so as to be less than the thickness of the fat layer. Measurements on the forearms of four males and one female were also carried out to determine μ_a and μ_s' of the muscle. The fibers were in contact with the extensor site of the right forearm placed on a desk. The separation of the source and

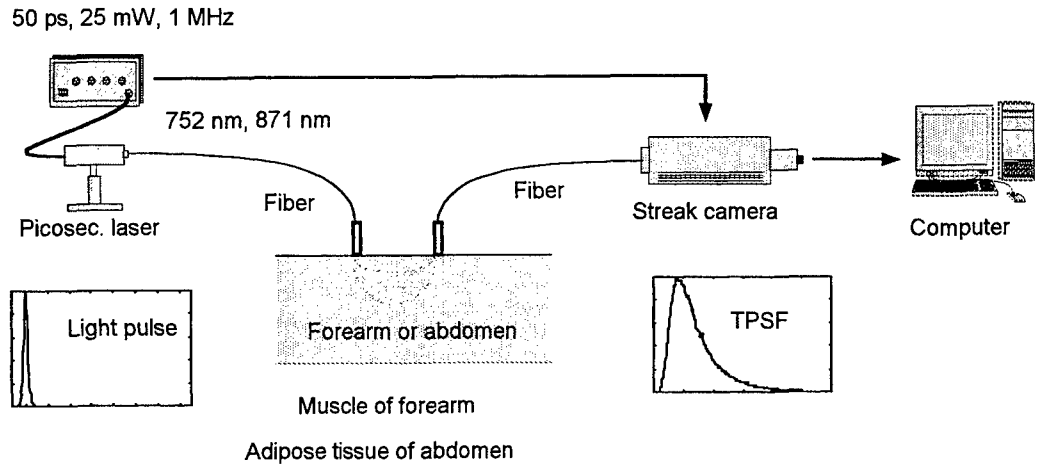

Fig. 5 Experimental setup for the measurement of TPSF.

detector fibers was 25 mm.

Absorption and reduced scattering coefficients were determined by fitting the measured TPSFs with those obtained by Monte Carlo simulation, which consisted of the skin, fat and muscle layers. The thickness of the fat layer of the model was set to be the same as that measured on each subject using ultrasonography. Coefficients μ_a and μ_s' of the skin were taken from the literatures[9,10]. First, the coefficients of the adipose tissue were determined using the TPSFs measured on the abdomens. After updating the optical properties of a fat layer of the model, μ_a and μ_s' of the muscle layer in each subject were determined by repeating the simulation.

4.2. Results

4.2.1. Optical properties of adipose and muscle tissues

Figure 6 (a) shows an example of the TPSF measured on the abdomen of one of the subjects at 752 nm. The TPSF obtained from the Monte Carlo simulation is also depicted by a solid line in this figure. The values of μ_a determined for the adipose tissue were 0.003–0.004 mm^{-1}at both wavelengths, and those of μ_s' were 1.1–1.15 mm^{-1} at 752 nm and 0.98–1.1 mm^{-1} at 871 nm. From these values, we chose the following values and used them in the simulation for determining the optical properties of muscle: μ_a =0.003 mm^{-1} and μ_s' =1.1 mm^{-1} at 752 nm, and μ_a =0.004 mm^{-1} and μ_s' =1.0 mm^{-1} at 871 nm.

Figure 6 (b) shows an example of the TPSF obtained from the forearm at 752nm. Table 1 shows μ_a and μ_s' of the forearm determined from the TPSF of each subject. As summarized in Table 1, μ_a and μ_s' of muscle determined in this study show only a small variation regardless of the thickness of the fat layer. These results indicate that the optical properties of muscle without the influence of a fat layer can be determined using by our method, although the uniqueness of a combination of μ_a and μ_s' must be quantitatively examined in further studies.

4.2.2. CW-NIRS algorithm

Using the mean values of μ_a and μ_s' shown in Table 1, we obtained the mean optical pathlenghts of 110 and 98 mm at 752 and 871 nm, respectively. Substituting these pathlengths and the absorption coefficients into equations (19) and (20), the nonlinear algorithm is readily obtained. Before applying this algorithm to measured ΔOD, it must be corrected by the thickness of the fat layer. The corrected ΔOD is thus equivalent to ΔOD, which is observed in a homogeneous muscle tissue.

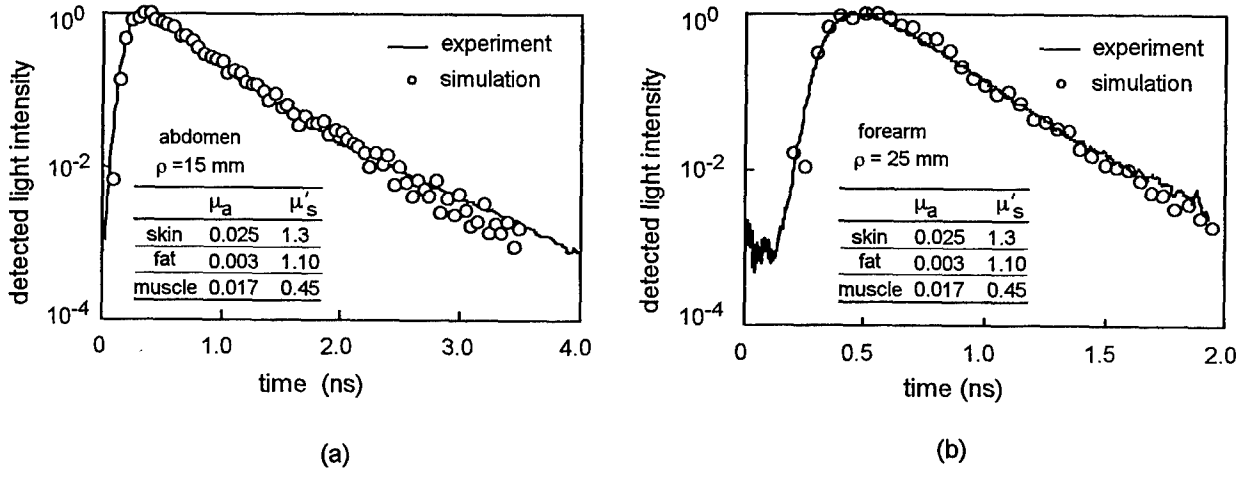

Fig. 6 Profiles of the TPSF measured on the abdomen (a) and forearm (b) of one of the subjects at 752 nm. Solid lines indicate fitting curves obtained from Monte Carlo simulation, in which absorption and scattering coefficients listed in tables were used.

Table 1 Optical properties of muscles obtained from *in vivo* measurements on the forearms of 5 subjects.

subject	h_f (mm)	μ_a (mm^{-1})		μ'_s (mm^{-1})	
		752 nm	871 nm	752 nm	871 nm
1	3.2	0.017	0.019	0.45	0.40
2	5.1	0.019	0.021	0.46	0.42
3	4.2	0.019	0.021	0.46	0.41
4	2.3	0.017	0.020	0.44	0.40
5*	2.8	0.015	0.017	0.45	0.42
mean ± SD	3.5± 1.1	0.017± 0.001	0.020± 0.002	0.45± 0.008	0.41± 0.01

*female

Therefore, an algorithm based on tissue homogeneity can be applied to corrected ΔOD, and the quantitative change in oxygenation can be obtained.

However, there are some limitations to CW-NIRS. The optical properties around an operating point must be known in advance. If these are known, ΔHbO_2 and ΔHb can be accurately estimated by using the nonlinear algorithm, as was verified by the results of the phantom experiments, but the values know before measurement are average values of different subjects. Lin et al.[11] estimated that the error of linear approximation is less than 10% when the operating point of μ_a is inappropriately set by ±0.005 mm^{-1} from a true value and that this error is much less than that resulting from the influence of fat layer. The error, when using the nonlinear algorithm, is much smaller than that of linear approximation, only if an adequate operating point is obtained. If not, the error might not be substantially improved even by the nonlinear algorithm.

One of the most practical solutions to the above-mentioned problem is to introduce spatially resolved (SR) NIRS, which gives the absolute value of μ_a if μ_s' is known. CW-NIRS and SR-NIRS are much more simplified and definitely less costly than intensity-modulated or time-resolved spectroscopy, although these sophisticated techniques enable the determination of both μ_a and μ_s'. In addition, real-time monitoring is possible only by using CW-NIRS or SR-NIRS, as inferred from the actual tedious procedures for obtaining μ_a and μ_s' described in the previous section. Complementary *in vivo* studies on the optical properties of tissues under various conditions using these different techniques should lead to realization of more quantitative measurement of tissue oxygenation using NIRS.

5. CONCLUSIONS

Equations for CW-NIRS algorithms using linear approximation and taking into account the nonlinear relationship between change in optical density and change in absorption coefficient were derived using the theoretical mean optical pathlength. The validity of these theoretical algorithms was examined on the basis of results obtained by phantom experiments. It was verified that the nonlinear algorithm is applicable to a wider range of absorption coefficients than is the linear algorithm if the initial operating point is appropriately given. To determine coefficients of the algorithms, the optical properties of muscle were measured using time-resolved spectroscopy by taking into account the influence of an overlying fat layer. In spite of the preliminary nature of our study, absorption and scattering coefficients were successfully obtained regardless of different thicknesses of the fat layer, and the coefficients of the algorithms were determined.

ACKNOWLEDGMENT

This research was supported in part by Grant-in-Aid for Scientific Research from the Ministry of Education, Science and Culture of Japan.

REFERENCES

1. S. Homma, T. Fukunaga, and A. Kagaya, "Influence of adipose tissue thickness on near infrared spectroscopic signal in the measurement of human muscle," *J. Biomedical Optics.*, **1**, pp. 418-424, 1996.
2. K. Yamamoto, M. Niwayama, T. Shiga, L. Lin, N. Kudo, and M. Takahashi, "Accurate NIRS measurement of muscle oxygenation by correcting the influence of a subcutaneous fat layer," *Proc. SPIE*, **3194**, pp. 166-173 1998.
3. K. Yamamoto, M. Niwayama, T. Shiga, L. Lin, N. Kudo, and M. Takahashi, "A near-infrared muscle oximeter that can correct the influence of a subcutaneous fat layer," *Proc. SPIE*, **3257**, pp. 145-155, 1998.
4. L. Lin, M. Niwayama, T. Shiga, N. Kudo, M. Takahashi, and K. Yamamoto, "Two-layered phantom experiments for characterizing the influence of a fat layer on measurement of muscle oxygenation using NIRS," *Proc. SPIE*, **3257**, pp. 156-166, 1998.
5. M. Niwayama, L. Lin, J. Shao, T. Shiga, N. Kudo, and K. Yamamoto, "Quantitative measurement of muscle oxygenation by NIRS: Analysis of the influences of a subcutaneous fat layer and skin," *Proc. SPIE*, **3597**, pp. 291-299, 1999.
6. D. T. Delpy, M. Cope, P. Zee, S. Arridge, S. Wray, and J. Wyatt, " Estimation of optical pathlength through tissue from direct time of flight measurement, " Phys. Med. Biol., **33**: 1433/1442 (1988)
7. S. J. Matcher, C. E. Elwell, C. E. Cooper, M. Cope, and D. T. Delpy, "Performance comparison of several published tissue near-infrared spectroscopy algorithms," *Analytical Biochemistry*, **227**, pp. 54-68, 1995.
8. H. Liu, D. A. Boas, Y. Zhang, A. G. Yohd and B. Chanc, " Determination of optical properties and blood oxygenation in tissue using continuous NIRS light," Phys. Med. Biol., **40**, 1983/1993 (1995)
9. A. Kienle, L. Lilge, M. S. Patterson, B. C. Wilson, R. Hibst and R. Steiner, "Investigation of Multi-Layered Tissue with *In-vivo* Reflectance Measurements," *Proc. SPIE*, **2326**, pp. 212-221, 1994.
10. C. R. Simpson , M. Kohl, M. Essenpreis and M. Cope, "Near-infrared optical properties of *ex vivo* human skin and subcutaneous tissues measured using the Monte Carlo inversion technique," *Phys. Med. Biol.* **43**: 2465-2478, 1998.
11. L. Lin, M. Niwayama, T. Shiga, N. Kudo, M. Takahashi and K. Yamamoto, "Influence of a fat layer on muscle oxygenation measurement using near-IR spectroscopy: quantitative analysis based on two-layered phantom experiments and Monte Carlo simulation," *Frontiers Med. Biol. Engng.*, **10** (in press).